Computational Methods for Reversed-Field Equilibrium

John K. Boyd
Steven P. Auerbach
Peter A. Willmann
Herbert L. Berk
Brendan McNamara

MASTER

This paper was prepared for submittal to
1980 Sherwood Theory Meeting
University of Arizona
Tucson, Arizona
April 23-25, 1980

April 15, 1980

Lawrence
Livermore
Laboratory

TABLE OF CONTENTS

Page

COMPUTATIONAL METHODS FOR REVERSED-FIELD EQUILIBRIUM*

J. K. Boyd, S. P. Auerbach, P. A. Willmann, H. L. Berk, and B. McNamara

Lawrence Livermore Laboratory, University of California,
Livermore, CA 94550

ABSTRACT

Investigating the temporal evolution of reversed-field equilibrium
caused by transport processes requires the solution of the Grad-Shafranov
equation and computation of field-line-averaged quantities. The technique for
field-line averaging and the computation of the Grad-Shafranov equation are
presented. Application of Green's function to specify the Grad-Shafranov
equation boundary condition is discussed. Hill's vortex formulas used to
verify certain computations are detailed. Use of computer software to
implement computational methods is described.

INTRODUCTION

The problem of reversed-field transport and equilibrium involves
computating field-line-averaged quantities and solving the Grad-Shafranov
equation. The methods used are described in the first part of this report and
the software implementation in the second part.

The first part describes the technique for field-line averaging, the tri-diagonal solution of the averaged Grad-Shafranov equation, the Incomplete Cholesky Conjugate Gradient (ICCG) solution of the two-dimensional Grad-Shafranov equation, and the application of Green's function to obtain boundary conditions. The computations of field-line-averaged functions are verified by using the Hill's vortex, analytic, reversed-field equilibrium. Because the use of Hill's vortex is widespread, the analytic formulas for pertinent transport and equilibrium functions are presented. Graphs of these functions versus flux are also included. These may be compared with other equilibria or with a Hill's vortex after it has evolved by transport. The second part of this work details the use of subroutines to implement our computational methods. The ICCG method is generally applicable to problems requiring the inversion of a matrix having five or more bands. An efficient assembly-language version of the five-band algorithm is available for users of the Magnetic Fusion Energy Computer Center's Cray 1 computer. All other subroutines are in FORTRAN. Several techniques used to reduce run time to one-fourth that for standard FORTRAN are discussed for the ICCG method.

I. METHODS AND HILL'S VORTEX SOLUTION

The central equation to be solved is Ampere's law combined with force balance in cylindrical coordinates. The general relation is the Grad-Shafranov equation,

$$\Delta^* \psi = - 4\pi r^2 p' - ff' \quad . \tag{1}$$

The toroidal, magnetic induction is f/r, and p is the pressure. Both p and f are functions of ψ where $\vec{B} = \nabla\psi \times \nabla\theta + f\nabla\theta$. The poloidal induction, $\vec{B}_p$, is $\nabla\psi \times \nabla\theta$. The average of (1) divided by r^2 is,

$$\frac{d}{dV} \left(K \frac{d\psi}{dV} \right) = - 4\pi p' - ff' \left\langle \frac{1}{r^2} \right\rangle \quad , \tag{2}$$

where

$$K = \left\langle \frac{|\nabla_V|^2}{r^2} \right\rangle .$$

Brackets denote an average over a flux surface. For a general function X,

$$\langle X \rangle = \int X \, \frac{d\ell}{B_p} \Big/ \int \frac{d\ell}{B_p} \quad .$$

An equilibrium is obtained when Eqs. (1) and (2) are self-consistently solved subject to constraints on $p(\psi)$ and $f(\psi)$ which enforce certain dynamical conservation laws.[1] It is then necessary to compute average quantities $\langle X \rangle$, and numerically solve (1) and (2).

A. FIELD-LINE AVERAGE

Let $[X] = \oint X \, d\ell/B_p$; then $\langle X \rangle$ is obtained as $\langle X \rangle = [X]/[1]$. It is only necessary to compute the un-normalized average. The function X, B_p, and flux, ψ, are specified on a rectangular grid which may be variable. The actual $[X]$ average is calculated along a constant ψ path. On the grid this is approximated by examining a grid cell and taking the integration path as a straight line between the ψ intersections of the grid-cell sides. The ψ intersection and the value of X at the intersection are obtained by linear interpolation. The value of X/B_p along the straight-line-integration path is taken to be the average of the values at the two intersections. The contribution of a grid cell to $[X]$ is the distance between ψ intersections multiplied by the sum of X/B_p at these two intersections. The factor of $1/2$ is absent because ψ contours are assumed to be symmetric about $z = 0$. The routine assumes it is only examining grid cells for z greater than zero. The value of $[X]$ is finally obtained by summing the contributions from all grid cells.

The procedure just described is a good approximation to $[X]$ except near the vortex point, where a ψ contour may intersect one side of a grid cell twice. To resolve this difficulty $\langle Y \rangle$ is defined to be a weighted sum of the numerical average and the analytic average obtained by using the Hill's vortex formulas described in a later section:

$$\langle X \rangle = e^{\alpha} \ \langle X \rangle_{analytic} + (1 - e^{\alpha}) \ \langle X \rangle_{numerical} \quad ,$$

$$\alpha = \left(\frac{\psi - \psi_v}{-0.2 \, \psi_v} \right)^2 \quad ,$$

where ψ_v is the flux value at the vortex point. At and near the vortex point $\langle X \rangle$ is almost entirely the analytical average. For $\psi - \psi_v$ greater than $-0.2 \, \psi_v$, $\langle X \rangle$ is almost entirely the numerical average.

B. TRIDIAGONAL SOLUTION OF THE AVERAGED GRAD-SHAFRANOV EQUATION

Equation (2) is the average Grad-Shafranov equation, with p and f arbitrary functions of ψ. It is iterated self-consistently with Eq. (1) to allow the imposition of a transport-determined flux value at the vortex point. To invoke adiabatic-equilibrium changes between transport steps, the following two relations are used:

$$p(\psi) = S(\psi) \left(\frac{d\psi}{dV} \right)^{\gamma} \quad , \tag{3}$$

$$f(\psi) = \frac{4\pi^2 \, q(\psi)}{\left\langle \dfrac{1}{r^2} \right\rangle} \frac{d\psi}{dV} \quad . \tag{4}$$

The left hand side of Eq. (2) is differenced in a conservative manner with a non-uniform mesh

$$\frac{d}{dV} \left(\kappa \frac{d\psi}{dV} \right) = \left(T_i^{(1)} + T_i^{(3)} \, h_1^2 \right) \psi_{i+1} + \left[T_i^{(3)} \left(h_2^2 - h_1^2 \right) - T_i^{(2)} - T_i^{(1)} \right] \psi_i$$

$$+ \left(T_i^{(2)} - h_2^2 \, T_i^{(3)} \right) \psi_{i-1} \quad . \tag{5}$$

The spacing between ψ_{i-1} and ψ_i is h_1, and the spacing between ψ_i and ψ_{i+1} is h_2. The $T_i^{(j)}$ functions are given below:

$$T_i^{(1)} = \frac{h_1^2}{h_2} \frac{\left(\kappa_{i+1} + \kappa_i \right)}{\left(h_1^2 \, h_2 + h_2^2 \, h_1 \right)} \quad ,$$

$$T_i^{(2)} = \frac{h_2^2 \left(K_i + K_{i-1}\right)}{h_1 \left(h_1^2 h_2 + h_2^2 h_1\right)} \quad ,$$

$$T_i^{(3)} = \frac{2 \left(h_2^2 - h_1^2\right) K_i}{\left(h_1^2 h_2 + h_2^2 h_1\right)^2} \quad .$$

The right hand side of Eq. (2) is written below:

$$R = - 4\pi \frac{\partial S}{\partial V} \left(\frac{d\psi}{dV}\right)^{\gamma-1} - 4\pi \gamma S \left(\frac{d\psi}{dV}\right)^{\gamma-2} \frac{d^2\psi}{dV^2}$$

$$- \frac{16\pi^4}{\left\langle \frac{1}{r^2} \right\rangle} q \left(\frac{dq}{dV} \frac{d\psi}{dV} + q \frac{d^2\psi}{dV^2} - \frac{q}{\left\langle \frac{1}{r^2} \right\rangle^2} \frac{d\left\langle \frac{1}{r^2} \right\rangle}{dV} \frac{d\psi}{dV}\right) \quad , \tag{6}$$

Define,

$$\sigma_i = \left[4\pi \gamma S \left(\frac{d\psi}{dV}\right)^{\gamma-2} + \frac{16\pi^4 q^2}{\left\langle \frac{1}{r^2} \right\rangle}\right]_i \frac{2}{h_1 h_2^2 + h_1^2 h_2} \quad , \tag{7}$$

$$\nu_i = \left[4\pi \frac{\partial S}{\partial V} \left(\frac{d\psi}{dV}\right)^{\gamma-2} + \frac{16\pi^4}{\left\langle \frac{1}{r^2} \right\rangle} q \frac{dq}{dV} - \frac{16\pi^4}{\left\langle \frac{1}{r^2} \right\rangle} \frac{q^2}{2} \frac{d\left\langle \frac{1}{r^2} \right\rangle}{dV}\right]_i \frac{1}{h_1^2 h_2 + h_1 h_2^2} \quad ; \tag{8}$$

then,

$$R_i = \left(- h_1 \sigma_i - h_1^2 \nu_i\right) \psi_{i+1} + \left(- h_2 \sigma_i + h_2^2 \nu_i\right) \psi_{i-1}$$

$$+ \left[\left(h_1 + h_2\right) \sigma_i + \left(h_1^2 - h_2^2\right) \nu_i\right] \psi_i \quad . \tag{9}$$

Using Eqs. (7), (8), and (9) in (5) yields,

$$A_i \; \psi_{i+1} + B_i \; \psi_i + C_i \; \psi_{i-1} = 0 \; , \tag{10}$$

where

$$A_i = T_i^{(1)} + T_i^{(3)} \; h_1^2 + h_1 \; \sigma_i + h_1^2 \; \nu_i \; ,$$

$$B_i = T_i^{(3)} \left(h_2^2 - h_1^2 \right) - T_i^{(2)} - T_i^{(1)} - \left(h_1 + h_2 \right) \sigma_i + \left(h_2^2 + h_1^2 \right) \nu_i \; ,$$

$$C_i = T_i^{(2)} - h_2^2 \; T_i^{(3)} + h_2 \; \sigma_i - h_2^2 \; \nu_i \; .$$

Equation (10) is homogeneous, because nonlinear terms such as $(d\psi/dV)^{\gamma-1}$ are treated as a product of two terms at different iteration levels,

$$\left(\frac{d\psi}{dV} \right)^{\gamma-1} = \left[\left(\frac{d\psi}{dV} \right)^{\gamma-2} \right]^n \left(\frac{d\psi}{dV} \right)^{n+1} \; .$$

Given ψ boundary values at the vortex point and separatrix, Eq. (10) is solved in the usual fashion:

$$\psi_{i+1} = E_i \; \psi_i + F_i \; ,$$

$$E_{i-1} = - C_i / \left(A_i \; E_i + B_i \right) \; ,$$

$$F_{i-1} = - A_i \; F_i / \left(A_i \; E_i + B_i \right) \; .$$

The function K has a logarithmic singularity at the separatrix. To avoid an infinity in the $T_i^{(1)}$ function one point from the separatrix, $K_{i+1} + K_i$ is replaced by $K_{i+1/2}$, obtained from a fit of interior K values assuming the following functional form,

$$K = a_1 V + a_2 V + \left(a_3 V + a_4 V^2\right) \ell n \left(1 - V\right)$$

$$+ \sum_{j=1}^{\ell} \sin j \pi V \left(c_j V + d_j V^2\right) \ ,$$

where V is normalized to the separatrix volume, and typically $\ell = 4$. The analytic derivative of this formula is used for dK/dV to obtain a smooth function that properly represents the $1/(1-V)$ singularity.

C. ICCG SOLUTION OF THE GRAD-SHAFRANOV EQUATION

The Grad-Shafranov equation in cylindrical coordinates is given below in Gaussian units,

$$\frac{\partial^2 \psi}{\partial r^2} - \frac{1}{r} \frac{\partial \psi}{\partial r} + \frac{\partial^2 \psi}{\partial z^2} = - \frac{4\pi}{c} r J \ , \tag{11}$$

where

$$J = c r p' + \frac{c}{4\pi r} ff' \ .$$

The ψ derivatives of pressure and toroidal flux are obtained by using Eqs. (3) and (4):

$$p' = \frac{dS}{dV} \left(\frac{d\psi}{dV}\right)^{\gamma-1} + \gamma S \left(\frac{d\psi}{dV}\right)^{\gamma-2} \frac{d^2\psi}{dV^2} \ ,$$

$$f' = \frac{4\pi^2}{\left\langle \frac{1}{r^2} \right\rangle} \left(\frac{dq}{dV} + q \frac{dV}{d\psi} \frac{d^2\psi}{dV^2} - \frac{1}{\left\langle \frac{1}{r^2} \right\rangle} \frac{d \left\langle \frac{1}{r^2} \right\rangle}{dV} \right).$$

As suggested by Grad, $d^2\psi/dV^2$ is expressed in terms of first derivative quantities by using the average equation and (6):

$$\frac{d^2\psi}{dV^2} = \left[-\frac{dK}{dV}\frac{d\psi}{dV} - 4\pi\frac{dS}{dV}\left(\frac{d\psi}{dV}\right)^{\gamma-1} \right.$$

$$\left. - \frac{16\pi^4}{\left\langle\frac{1}{r^2}\right\rangle} q\frac{d\psi}{dV}\left(\frac{dq}{dV} - \frac{1}{\left\langle\frac{1}{r^2}\right\rangle}\frac{d}{dV}\left\langle\frac{1}{r^2}\right\rangle\right)\right]\frac{1}{D} \quad,$$

$$D = K + 4\pi\gamma S\left(\frac{d\psi}{dV}\right)^{\gamma-2} + 16\pi^4\frac{q^2}{\left\langle\frac{1}{r^2}\right\rangle} \quad.$$

Applying central differences to Eq. (11) on a variable mesh yields

$$\epsilon_{ij}\psi_{i+1,j} + \psi_{ij} + \beta_{ij}\psi_{i-1,j} + \gamma_{ij}\psi_{ij+1} + \lambda_{ij}\psi_{ij-1}$$

$$= -\frac{4\pi}{c}\delta_{ij}r_i J_{ij} \quad, \tag{12}$$

where the coefficients for an r,z mesh are given below:

$$\delta_{ij} = \left\{ - 2\left[\Delta r_i + \Delta r_{i+1}\right]/R_i \right.$$

$$+ \left[\left(\Delta r_i\right)^2 - \left(\Delta r_{i+1}\right)^2\right]/S_i$$

$$\left. - 2\left[\Delta z_j + \Delta z_{j+1}\right]/T_j\right\}^{-1}$$

$$\alpha_{ij} = \delta_{ij}\left[2\Delta r_i/R_i - \left(\Delta r_i\right)^2/S_i\right]$$

$$\beta_{ij} = \delta_{ij}\left[2\Delta r_{i+1}/R_i + \left(\Delta r_i\right)^2/S_i\right]$$

$$\gamma_{ij} = \delta_{ij}\ 2\Delta z_j/T_j$$

$$\lambda_{ij} = \delta_{ij}\, 2\Delta z_{j+1}/T_j$$

$$R_i = \left(\Delta r_{i+1}\right)^2 \Delta r_i + \left(\Delta r_i\right)^2 \Delta r_{i+1}$$

$$S_i = r_i\, R_i$$

$$T_j = \left(\Delta z_{j+1}\right)^2 \Delta z_j + \left(\Delta z_j\right)^2 \Delta z_{j+1}$$

$$\Delta z_j = z_j - z_{j-1}$$

$$\Delta r_i = r_i - r_{i-1} \; .$$

The solution of the difference Eq. (12) is equivalent to the inversion of a matrix having five bands. The solution is obtained using a modification of the Incomplete Cholesky Conjugate Gradient Method (ICCG) devised by D. S. Kershaw.[2] The problem reduces to finding $\underline{\psi}$ given $\underline{\underline{A}}$ and $\underline{J}$ in Eq. (13),

$$\underline{\underline{A}}\, \underline{\psi} = -\frac{4\pi}{c}\, r\underline{J} \; . \tag{13}$$

After a lower, upper, triangular decomposition of matrix $\underline{\underline{A}}$, Eq. (13) becomes

$$\underline{\underline{L}}\; \underline{\underline{D}}\; \underline{\underline{U}}\; \underline{\psi} = -\frac{4\pi}{c}\, r\underline{J} \; . \tag{14}$$

The $\underline{\underline{L}}$, $\underline{\underline{U}}$, and $\underline{\underline{D}}$ matrices in Eq. (14) are given below:

$$L_{ji} = A_{ji} - \sum_{k=1}^{i-1} L_{jk}\, U_{ki}\, D_{kk} \; , \tag{15}$$

$$U_{ij} = A_{ij} - \sum_{k=1}^{i-1} L_{ik}\, U_{kj}\, D_{kk} \; , \tag{16}$$

$$D_{ii} = (U_{ii})^{-1} \; . \tag{17}$$

The grid is M by N, and the matrices are M × N by M × N. The five point difference scheme results in $\underline{\underline{A}}$ having five bands. The bands are then:

$$L_{i,i-1} = A_{i,i-1} \quad , \tag{18}$$

$$L_{i,i-M} = A_{i,i-M} \quad , \tag{19}$$

$$L_{ii} = A_{ii} - L_{ii-1} \, U_{i-1,i-1} \, D_{i-1,i-1} - L_{i,i-M} \, U_{i-M,i} \, D_{i-M,i-M} \quad , \tag{20}$$

$$U_{ii} = L_{ii} \quad , \tag{21}$$

$$U_{i,i+1} = A_{ii+1} \quad , \tag{22}$$

$$U_{i,i+M} = A_{i,i+M} \quad . \tag{23}$$

It is only necessary to compute L_{ii}. Eqs. (18) to (23) are used in the algorithm below:

$$\underline{S}^o = -\frac{4\pi}{c} \, r\underline{J} - \underline{\underline{A}} \, \underline{\psi} \tag{24}$$

$$\underline{p}^o = \underline{\underline{A}}^T \, (L \, D \, U)^{-T} \, (L \, D \, U)^{-1} \, S^o \quad , \tag{25}$$

$$a^i = \frac{\left[(L \, D \, U)^{-1} \, S^i, \, (L \, D \, U)^{-1} \, S^i\right]}{(p^i, \, p^i)} \quad , \tag{26}$$

$$\underline{\psi}^{i+1} = \underline{\psi}^i + a^i \, \underline{p}^i \quad , \tag{27}$$

$$\underline{S}^{i+1} = \underline{S}^i - a^i \, \underline{\underline{A}} \, \underline{p}^i \quad , \tag{28}$$

$$b^i = \frac{\left[(L\ D\ U)^{-1}\ S^{i+1},\ (L\ D\ U)^{-1}\ S^{i+1}\right]}{\left[(L\ D\ U)^{-1}\ S^i,\ (L\ D\ U)^{-1}\ S^i\right]} \quad , \tag{29}$$

$$\underline{p}^{i+1} = A^T\ (L\ D\ U)^{-T}\ (L\ D\ U)^{-1}\ \underline{S}^{i+1} + b^i\underline{p}^i \quad . \tag{30}$$

Operations such as $z = (L\ D\ U)^{-1}\ S^i$ are performed by using tridiagonal back substitution in three steps as follows:

$$Lx = S^i \quad ,$$

$$Dy = x \quad ,$$

$$Uz = y \quad .$$

The algorithm is iterated from Eq. (26) to Eq. (30) until the residual S^i is sufficiently small.

The five band ICCG method, Eqs. (18) to (30), is a mathematical operation and is therefore applicable to other physical situations in addition to the equilibrium problem. It may also be generalized to cases involving nine or more bands in the A matrix.

D. BOUNDARY CONDITION

The specification of the solution of Eq. (1) requires a boundary condition. A Green's function technique is used to obtain the boundary condition by summing the flux due to current rings. Each grid point where the current is non-zero is considered to be a current ring. The flux due to a current ring[3] is given by Eq. (31):

$$\psi(r,z) = \int\int dr'\ dz'\ G(r',\ z',\ r,z)\ J \quad , \tag{31}$$

where

$$G(r', z', r, z) = \frac{4}{c} \left\{ \sqrt{\frac{r'r}{k^2}} \left[\left(1 - \frac{1}{2} k^2\right) K(k) - E(k) \right] \right\}$$

$$k^2 = \frac{4 \, r'r}{(r' + r)^2 + (z - z')^2}$$

and $K(k)$ and $E(k)$ are elliptic integrals of the first and second kind, respectively. The analytic formula in Eq. (31) is approximated below:

$$\psi(r,z) = \frac{1}{4} \sum_{ij} \left[J_{ij} \, G\left(r_i, \, z_j, \, r,z\right) + J_{i-1,j} \, G\left(r_{i-1}, \, z_j, \, r,z\right) \right.$$

$$\left. + J_{i,j-1} \, G\left(r_i, \, z_{j-1}, \, r,z\right) + J_{i-1,j-1} \, G\left(r_{i-1}, \, z_{j-1}, \, r,z\right) \right] \Delta r_i \, \Delta z_j \quad.$$

The Green's function, $G(r_i, z_j, r,z)$, must be computed for each grid point, for all r,z where a boundary condition is required. Because it is necessary to read G from a disk, the change of the $z = 0$ boundary point is monitored during solution iteration, and all boundary values are recomputed only if there is a significant change at $z = 0$. Because of ymmetry the actual Green's function used for computation is $G(r', z', r,z) + G(r', -z', r,z)$.

E. HILL'S VORTEX FORMULAS

The Hill's vortex model[4] has been used to verify the ICCG solution of Eq. (1) and the computation of field-line averages. Relevant transport and equilibrium functions are given below in terms of the Hill model to allow comparison with other equilibria or with a Hill's vortex after it has evolved by transport.

The flux is expressed as a polynomial in r and z:

$$\psi = -\frac{r^2}{2} \left(\beta - \gamma z^2 - \frac{\delta}{6} r^2 \right) \quad. \tag{32}$$

The vortex point radius r_v, flux at the vortex point ψ_v, and total volume within the separatrix, V_s, may be calculated by using Eq. (32).

$$r_v = \left(\frac{3\beta}{\delta}\right)^{1/2} \quad,$$

$$\ddot{r}_v = -\frac{3}{4}\frac{\epsilon^2}{r} \quad,$$

$$V_s = 8^- \frac{\cdot}{\cdot} \left(\frac{r}{\cdot}\right)^{1/2} \quad.$$

The volume as a function of flux $V(\psi)$, the average quantities, and their derivatives are obtained as trigonometric integrals which are evaluated numerically by using Simpson's rule. For the average functions the following relation is used:

$$\frac{d\Gamma}{B}_p = \frac{dr}{v\gamma\,(2, + \epsilon\, r^2 - \frac{\lambda}{6}\, r^4)^{1/2}} \quad.$$

The analytic Hill formulas are given below with small b expansions (beneath each formula) where $b = (1 - \psi/\psi_v)^{1/2}$. The separatrix corresponds to $b = 1$ and the vortex point corresponds to $b = 0$.

$$V(\psi) = -\frac{3V_s\, b}{2\sqrt{2}} \int_0^\pi d\theta\, \cos\theta\, (1 - b\cos\theta)^{1/2} \tag{33}$$

$$V(b \approx 0) = \frac{3r}{8\sqrt{2}}\, V_s \left(b^2 + \frac{3}{32}\, b^4\right) \tag{34}$$

$$\frac{dV}{d\psi} = -\frac{3\sqrt{2}}{16}\frac{V_s}{\psi_v} \int_0^\pi \frac{d\theta}{(1 - b\cos\theta)^{1/2}} \tag{35}$$

$$\frac{dV}{d\psi}\,(b \approx 0) = -\frac{3-}{8\sqrt{2}}\frac{V_s}{\psi_v} \left(1 + \frac{3b^2}{16}\right) \tag{36}$$

$$\frac{d^2V}{d\psi^2} = \frac{3V_s}{32\sqrt{2}\,\psi_v^2}\frac{1}{b} \int_0^\pi d\theta\, \frac{\cos\theta}{(1 - b\cos\theta)^{3/2}} \tag{37}$$

$$\frac{d^2 V}{d\psi^2} (b \approx 0) = \frac{3V_s}{32\sqrt{2}\ \psi_v^2} \left(\frac{3\pi}{4} + \frac{105}{128} b^2 \right) \tag{38}$$

$$\frac{d^2\psi}{dV^2} = - \left(\frac{d\psi}{dV} \right)^3 \frac{d^2 V}{dV^2} \tag{39}$$

$$K = \left(\gamma + \frac{2\delta}{3} \right) V \frac{d\psi}{dV} \tag{40}$$

$$\frac{dK}{dV} = \left(\gamma + \frac{2\delta}{3} \right) \left(\frac{d\psi}{dV} + V \frac{d\psi}{dV} \frac{d^2 V}{d\psi^2} \right) \tag{41}$$

$$\left\langle \frac{1}{r^2} \right\rangle = - \frac{3\sqrt{2}}{16\psi_v} \frac{V_s}{r_v^2} \frac{d\psi}{dV} \int_0^\pi \frac{d\theta}{(1 - b \cos \theta)^{3/2}} \tag{42}$$

$$\left\langle \frac{1}{r^2} \right\rangle (b \approx 0) = \frac{1}{r_v^2} \left(1 + \frac{3}{4} b^2 + \frac{131}{64} b^4 \right) \tag{43}$$

$$\frac{d}{dV} \left\langle \frac{1}{r^2} \right\rangle = \frac{d^2\psi}{dV^2} \frac{dV}{d\psi} \left\langle \frac{1}{r^2} \right\rangle + \frac{9\sqrt{2}}{64\psi_v^2} \frac{V_s}{r_v^2 b} \left(\frac{d\psi}{dV} \right)^2 \int_0^\pi \frac{d\theta \cos \theta}{(1 - b \cos \theta)^{5/2}} \tag{44}$$

$$\frac{d}{dV} \left\langle \frac{1}{r^2} \right\rangle (b \approx 0) = \frac{2\sqrt{2}}{\pi} \frac{1}{V_s r_v^2} \left(1 + \frac{251}{48} b^2 \right) \tag{45}$$

$$\langle r^2 \rangle = \frac{V_s}{\beta} \frac{3}{\sqrt{8}} \frac{d\psi}{dV} \int_0^\pi d\theta\ (1 + b \cos \theta)^{1/2} \tag{46}$$

$$\langle r^2 \rangle (b \approx 0) = \frac{d\psi}{dV} \frac{V_s}{\beta} \frac{3\pi}{\sqrt{8}} \left(1 - \frac{b^2}{16} \right) \tag{47}$$

$$\frac{d}{dV} \langle r^2 \rangle = \frac{dV}{d\psi} \frac{d^2\psi}{dV^2} \langle r^2 \rangle - \left(\frac{d\psi}{dV} \right)^2 \frac{V_s}{\beta} \frac{3}{4} \frac{1}{\psi_v b\sqrt{8}} \int_0^\pi \frac{d\theta \cos \theta}{(1 + b \cos \theta)^{1/2}} \tag{48}$$

$$\frac{d}{dV} \langle r^2 \rangle \, (b \approx 0) = \frac{dV}{d\psi} \frac{d^2 \psi}{dV^2} \quad \langle r^2 \rangle \; + \left(\frac{d\psi}{dV}\right)^2 \frac{V_s}{\beta} \frac{3}{4} \frac{1}{\psi_v \sqrt{\zeta}} \left(\frac{1}{4} + \frac{15}{128} \, b^2\right) \tag{49}$$

Let

$$\zeta = \frac{2\psi\delta}{3\beta(1 + b \cos \theta)} + \frac{\beta}{2} (1 + b \cos \theta) ,$$

$$\left\langle \frac{1}{B^2} \right\rangle = 2 \cdot \left(\frac{2}{\gamma\beta}\right)^{1/2} \frac{d\psi}{dV} \int_0^{\pi} \frac{d\theta}{(1 + b \cos \theta)^{1/2} (\zeta^2 - 2\gamma \, \psi_v \, b^2 \sin^2 \theta)} \tag{50}$$

$$\left\langle \frac{1}{B^2} \right\rangle (b \approx 0) = 2\pi \left(\frac{2}{\gamma\beta}\right)^{1/2} \frac{d\psi}{dV} \frac{1}{\beta} \left(\frac{2.3748}{b^2} + 0.38349 + 0.2 \, b^2\right) \tag{51}$$

$$\frac{d}{dV} \left\langle \frac{1}{B^2} \right\rangle = \frac{dV}{d\psi} \frac{d^2_\perp}{dV^2} \left\langle \frac{1}{B^2} \right\rangle \; + \frac{}{b \, \psi_v} \left(\frac{2}{\gamma\beta}\right)^{1/2} \left(\frac{d\psi}{dV}\right)^2$$

$$\int_0^{\pi} \frac{1}{(1 + b \cos \theta) \, (\zeta^2 - 2\gamma \, \psi_v \, b^2 \sin^2 \theta)^2}$$

$$\cdot \left[\frac{\cos \theta}{2(1 + b \cos \theta)^{1/2}} \left(\zeta^2 - 2\gamma \, \dot{\psi}_v \, b^2 \sin^2 \theta\right) \right.$$

$$+ (1 + b \cos \theta)^{1/2} \left\{ 2\zeta \left[\left(\frac{\beta}{2} - \frac{2\psi\delta/3\beta}{(1 + b \cos \theta)^2}\right) \cos \theta \right.\right.$$

$$\left.\left.- \frac{2\delta/3\beta}{1 + b \cos \theta} \, 2b \, \psi_v \right] - 4b \, \gamma \, \dot{\psi}_v \, \sin^2 \theta \right\} \right] d\theta , \tag{52}$$

$$\frac{d}{dV} \left\langle \frac{1}{B^2} \right\rangle (b \approx 0) = \frac{dV}{d\psi} \frac{d^2 \psi}{dV^2} \left\langle \frac{1}{B^2} \right\rangle + \frac{2\pi}{\beta} \left(\frac{2}{\gamma\beta}\right)^{1/2} \frac{d\psi}{dV} \left(\frac{-4.7496}{b^3} + 0.4 \, b\right) \tag{53}$$

$$\langle B^2 \rangle = \left(\frac{d\psi}{dV}\right)^2 K , \tag{54}$$

$$\frac{d}{dV} \langle B^2 \rangle \approx \left(\frac{d\psi}{dV}\right)^2 \frac{dK}{dV} + 2K \frac{d\psi}{dV} \frac{d^2\psi}{dV^2} \; . \tag{55}$$

The magnitude of the magnetic field $|B|$ around a flux surface is computed by obtaining the distance along a flux surface ℓ, and using the definition of $|B|$ below.

$$|B| = \left[\left(\frac{2\psi}{r^2} + \frac{\delta r^2}{6}\right)^2 + \gamma \left(2\psi + \beta r^2 - \frac{\delta}{6} r^4\right)\right]^{1/2} . \tag{56}$$

The trigonometric integral for $\int d\ell$ has an integrable singularity at $\theta = \pi$ which causes numerical difficulty. To resolve this problem $\int d\ell$ is computed in two parts. The first part of the integral is in z,

$$\int_0^{\ell_1} d\ell = \int_0^{z_1} \left[1 + \frac{\gamma\left(2\psi + \beta r^2 - \frac{\delta}{6} r^4\right)}{\left(\frac{2\psi}{r^2} + \frac{\delta}{6} r^2\right)^2}\right]^{1/2} dz \; , \tag{57}$$

with

$$r^2 = \left\{\frac{\beta}{2} - \frac{\gamma z^2}{2} - \left[\left(\frac{\beta}{2} - \frac{\gamma z^2}{2}\right)^2 + \frac{\delta}{3} \psi\right]^{1/2}\right\} \frac{6}{\delta}$$

used in Eqs. (56) and (57). The second part of $\int d\ell$ is an angular integral,

$$\int_{\ell_1}^{\ell_2} d\ell = -\frac{1}{(2\gamma\beta)^{1/2}} \int_{\theta_1}^{\theta_2} \frac{d\theta}{(1 + b \cos \theta)^{1/2}} \left(\zeta^2 - 2\gamma\psi_v b^2 \sin^2 \theta\right)^{1/2} \; , \tag{58}$$

with

$$r^2 = \frac{3\beta}{\delta} (b \cos \theta + 1)$$

used in Eq. (56).

Functions given by Eqs. (33) to (58) are plotted in Figs. 1 to 10 for three aspect ratios with $\psi_v = -1$ and $r_v = 1/\sqrt{2}$. The flux ranges from -1 to 0 from the vortex point to the separatrix, and ψ is zero at $r = 1$ and $z = 0$. For all cases $\beta = 8$, and $\delta = 48$ in Eq. (32). Plots with three curves labelled A, B, C refer to $\gamma = 4$, 8, and 16, respectively. These values of γ correspond to a ratio of radial to axial separatrix distance squared, E, equal

of 0.5, 1 and 2. To avoid singularities the range of ψ is restricted to -0.95
to -0.05.

Figures 1a, b, and c are contour plots showing the different geometries
for the three E values. Case A, Fig. 1a, is prolate; case B, Fig. 1b, is
spherical; and case C, Fig. 1c, is oblate.

The volume, $V(\psi)$, is plotted in Fig. 2a. The prolate geometry, case A,
has the greatest volume at any value of flux. The oblate case, C, has the
least volume and the spherical case, B, is intermediate between these two
extremes. The volume derivative of ψ, $d\psi/dV$ is plotted in Fig. 2b. The
greatest to least $d\psi/dV$ occur for the oblate, spherical and prolate cases,
respectively. Each curve would plunge to zero at $\psi = 0$, the separatrix, if
the plotting range were extended. This sudden change in value is a
consequence of the logarithmic singularity of K mentioned earlier and the fact
K $d\psi/dV$ is proportional to the total enclosed current. Because the total
current is finite and K is singular, $d\psi/dV$ must go to zero. Figure 2c,
$d^2\psi/dV^2$, dramatically illustrates the sudden rate of change of the slope
of $d\psi/dV$ near $\psi = 0$. The relative magnitude of $d^2\psi/dV^2$ for the three
cases is prolate, spherical and oblate. This is the opposite of the ordering
for $d\psi/dV$.

Figure 3a is a plot of $\langle 1/r^2 \rangle (\psi)$. This function goes to infinity at
$\psi = 0$; and consequently $d/dV \langle 1/r^2 \rangle$ in Fig. 3b and $d/d\psi \langle 1/r^2 \rangle$ in Fig. 3c
rise sharply near $\psi = 0$. Figures 3a and 3c show $\langle 1/r^2 \rangle$ and $d/d\psi \langle 1/r^2 \rangle$
are both independent of E for Hill's vortex.

Figures 4a, b, and c are plots f $K(\psi)$, dK/dV, and $dK/d\psi$, respectively.
The greatest to least value at a given flux occurs for prolate, spherical and
oblate geometry for each plot. The weak singularity at $\psi = 0$ is illustrated
by the rapid increase of dK/dV or $dK/d\psi$ near $\psi = 0$. Because the poloidal
field is zero at the vortex point, K = 0 at $\psi = -1$, as shown in Fig. 4a.

Figures 5a, b, and c are plots of $\langle r^2 \rangle$, $d/dV \langle r^2 \rangle$ and $d/d\psi \langle r^2 \rangle$.
Figures 5a and 5c show that $\langle r^2 \rangle$ and $d/d\psi \langle r^2 \rangle$ do not depend on E. This
is consistent with Eqs. (46) and (48). The greatest to least magnitude of
$d/dV \langle r^2 \rangle$ at fixed ψ occurs for prolate, spherical and oblate geometry,
respectively.

Figure 6a is a plot of $\langle 1/B^2 \rangle$ as a function of flux. Because $|B|$ is
zero at the vortex point $\langle 1/B^2 \rangle$ goes to infinity at $\psi = -1$ as indicated.
As the proximity of $d/dV \langle 1/B^2 \rangle$ to zero in Fig. 6b shows, $\langle 1/B^2 \rangle$ is
relatively constant for $-0.8 < \psi < 0$. The greatest to least magnitude of

$\langle 1/B^2 \rangle$ at constant ψ occurs for prolate, spherical and oblate geometry, respectively. Figure 6b shows $d/dV \langle 1/B^2 \rangle$ has a very weak dependency on E. Figure 6c shows a crossover point for $d/d\psi \langle 1/B^2 \rangle$. For ψ less than -0.2 the greatest to least value occurs for oblate, spherical and prolate geometry. For ψ greater than -0.2 the order becomes prolate, spherical and oblate.

Figure 7a shows $\langle B^2 \rangle$ with the greatest to least value occurring for oblate, spherical and prolate geometry, respectively. Because $|B|$ is zero at the vortex point $\langle B^2 \rangle$ is also zero at $\psi = -1$ as indicated by Fig. 7a. The existence of a maximum value of $\langle B^2 \rangle$ for each E value leads to a crossover point for $d/dV \langle B^2 \rangle$ and $d/d\psi \langle B^2 \rangle$ as shown in Figs. 7b and 7c. For $\psi < -0.11$ the greatest to least value of the derivative occurs for oblate, spherical, and prolate geometry, respectively. For $\psi > -0.11$ the order becomes prolate, spherical, and oblate.

Figures 8, 9, and 10 are plots of $|B|$ as a function of distance around a flux surface beginning at $z = 0$ below the vortex point. The main features of $|B|$ for Hill's vortex are the positions where $|B| = 0$ at the vortex point and separatrix, and the $|B|$ maximums above and below the vortex point. On a particular flux surface $|B|$ has the same value at the two radial positions at $z = C$. The basic feature of $|B|$ shown in Figs. 8, 9, and 10 is the existence of two minimums and two maximums around a flux surface. For the prolate geometry Fig. 8, the spherical geometry Fig. 9, and the oblate geometry Fig. 10, $|B|$ is plotted for $\psi = -0.8, -0.6, -0.4$, and -10^{-4}. The important difference between these plots is the ratio of maximum to minimum $|B|$, R, summarized for various ratios of radial to axial separatrix distance squared, E, and flux below.

ψ	E		
	0.5	1.0	2.0
- 8	2.84	2.06	1.48
-.6	2.97	2.29	1.58
-.4	3.26	2.38	1.74
-.0001	30.7	20.0	19.8

At constant E, R increases as ψ increases, moving from the vortex point toward the separatrix. The minimum $|B|$ exactly on the separatrix is zero, so R goes to infinity at $\psi = 0$. This accounts for the large R values for $\psi = -0.0001$. For a fixed value of flux, R decreases as E increases. The oblate geometry has the smallest values of R.

II. COMPUTATIONAL IMPLEMENTATION

A. FIELD-LINE AVERAGE

The $|\chi|$ operation discussed in Sec. IA is performed by subroutine FLINAV. The calling sequence is given below:

CALL FLINAV (SI, F, IR, IZ, IRD, IRZ, R, Z, HTS, N, XINT).

The subroutine computes N averages of function F and returns values in array, XINT. Function F is considered to be the entire integrand, i.e., χ/B_p for the average of Sec. IA. Computation proceeds on a rectangular grid bounded by $Z(1)$, to $Z(IZ)$ and $R(1)$ to $R(IR)$. Averaging is assumed to be done on flux heights symmetric about $z = 0$. An explanation of the calling arguments follows:

1.	SI(IRD, IZD)	Array of flux values. Averages are performed along constant SI heights. (INPUT)
2.	F(IRD, IZD)	Array of function values to be averaged. (INPUT)
3.	IR	The maximum radial index over which averaging occurs. This must be less than or equal to IRD. (INPUT)
4.	IZ	The maximum axial index over which averaging occurs. This must be less than or equal to IZD. (INPUT)
5.	IRD	First dimension of arrays F and SI. (INPUT)
6.	IZD	Second dimension of arrays F and SI. (INPUT)

7.	R(IR)	Array of radial grid positions. (INPUT)
8.	Z(IZ)	Array of axial grid positions. (INPUT)
9.	HTS(N)	The heights along which averages are computed. (INPUT)
10.	N	The number of averages to be computed. (INPUT)
11.	XINT(N)	Array of average values. (OUTPUT)

B. FIVE BAND ICCG

The solution of Eq. (12) is obtained by using six subroutines SETICC, CORICC, BACKL, BACKU, DINV, and MATMUL. The user need only call subroutines SETICC and CORICC. Subroutine SETICC is called once to compute band 3 given in Eq. (20) and to compute the initial vectors $\underline{S}$ and $\underline{P}$ given by Eqs. (24) and (25). Subroutine CORICC performs one loop through the ICCG algorithm given by Eqs. (26) to (30). Assume the equation to be solved is

$$A \underline{x} = \underline{y} , \tag{59}$$

where the five bands of matrix $\underline{A}$ are as shown in Fig. 11. The z,r grid is dimensioned IZDIM by IRDIM as shown in Fig. 12. The main diagonal of matrix A has a length equal to the number of grid points, IZDIM times IRDIM.

Vector $\underline{x}$ elements then refer to grid points $[z(i), R(1) , ... z(1),$ $R(IRDIM)], . . . [z(2), R(1)], . . . [z(2), R(IRDIM)].$ In other words, $\underline{x}$ consists of consecutive columns of the grid. Before discussing the calling arguments of SETICC and CORICC it is necessary to describe the construction of the five bands, and the $\underline{y}$ vector of Eq. (59). The description is given in terms of α_{ij}, β_{ij}, γ_{ij}, λ_{ij}, and δ_{ij} of Eq. (12) and grid boundary values denoted ψ_b. Assume arrays A1, A2, A3, A4, A5, X, and Y are dimensioned IRDIM by IZDIM.

Band 1

Interior grid points,

A1 $(i, j) = \lambda_{i\,j+1}$

$i = 2$, IRDIM-1

$j = 1$, IZDIM-1

Axis grid points,

A1 $(1, j) = 0$

$j = 1$, IZDIM

Boundary at maximum radial position,

A1 (IRDIM, j) = 0

$j = 1$, IZDIM

Boundary at maximum axial position,

A1 (i, IZDIM-1) = 0

$i = 2$, IRDIM-1

Band 2

Interior grid points,

A2 $(i, j) = \beta_{i+1,j}$

$i = 1$, IRDIM-1

$j = 1$, IZDIM-1

Axis grid points,

A2 (IRDIM, j) = 0

$j = 1$, IZDIM-1

Boundary at maximum radial position,

A2 (IRDIM-1, j) = 0

$j = 1$, IZDIM

Boundary at maximum axial position,

A2 (i - 1, IZDIM) = 0

$i = 2$, IRDIM-1

Premultiply band times axis boundary condition, where

ψ_b $(1, j) = 0$,

A2 $(1, j) = 0$

$j = 1$, IZDIM-1

Band 3

    A3 $(i, j) = 1$ $i = 1$, IRDIM
                                                     $j = 1$, IZDIM

Band 4

    Interior grid points,
    A4 $(i, j) = \alpha_{ij}$ $i = 2$, IRDIM
                                                   $j = 1$, IZDIM

    Axis grid points,
    A4 $(1, j) = 0$ $j = 1$, IZDIM

    Boundary at maximum radial position,
    A4 (IRDIM, $j) = 0$ $j = 1$, IZDIM

    Boundary at maximum axial position,
    A4 $(i$, IZDIM$) = 0$ $i = 2$, IRDIM $- 1$

    The band times the boundary condition is premultiplied and put on the
right hand side so,

    A4 (IRDIM-1, $j) = 0$. $j = 1$, IZDIM $- 1$

Band 5

    Interior grid points,
    A5 $(i, j) = \gamma_{ij}$ $i = 2$, IRDIM
                                                   $j = 1$, IZDIM

    Axis grid points,
    A5 $(1, j) = 0$ $j = 1$, IZDIM

    Boundary at maximum radial position,
    A5 (IRDIM, $j) = 0$ $j = 1$, IZDIM

The band times the boundary condition is premultiplied and put on the right hand side so

$$A5 \ (i + 1, \ IZDIM-1) = 0. \qquad\qquad i = 1, \ IRDIM - 2$$

Right hand side,
$$Y \ (i, \ j) = - \ 4\pi/c \ q_{ij} r_i l_{ij} \qquad\qquad i = 2, \ IRDIM - 1$$
$$j = 1, \ IZDIM$$

Axis grid points,
$$Y \ (1, \ j) = q_b \ (1, \ j) \qquad\qquad j = 1, \ IZDIM$$

Boundary at maximum radial position,
$$Y \ (IRDIM, \ j) = q_b \ (IRDIM, \ j) \qquad\qquad j = 1, \ IZDIM$$

Boundary at maximum axial position,
$$Y \ (i, \ IZDIM) = q_b \ (i, \ IZDIM) \qquad\qquad i = 2, \ IZDIM - 1$$

Note the following step of putting band times boundary condition on the right hand side must be performed prior to zeroing bands 2, 4, and 5.

$$z \ (IRDIM-1, \ j) = Y \ (IRDIM - 1, \ j)$$

$$Y \ (IRDIM-1, \ j) = - \ A4 \ (IRDIM-1, \ j)$$
$$+ \ z(IRDIM-1, \ j) \qquad\qquad j = 1, \ IZDIM - 1$$

$$z \ (i + 1, \ IZDIM-1) = Y \ (i + 1, \ IZDIM-1)$$
$$i = 1, \ IRDIM - 2$$

$$Y \ (i + 1, \ IZDIM-1) = z \ (i + 1, \ IZDIM-1)$$
$$- \ A5 \ (i + 1, \ IZDIM-1) \ Y \ (i + 1 + IRDIM,$$
$$IZDIM-1) \qquad\qquad i = 1, \ IRDIM-2$$

The calling sequence and arguments for subroutines SETICC and CORICC are now given:

CALL SETICC (A1, A2, A3, A4, A5, B, P, R, T1, T2, U3, X, Y, MN, M).

Subroutine arguments A1, A2, A3, A4, A5, P, R, T1, T2, U3, X, and Y are one-dimensional arrays of length MN, where MN is the total number of grid points, IZDIM times IRDIM. The band 3 to band 5 offset is M which would be IRDIM for Fig. 12.

1. - 5.		The first five arguments are arrays containing bands 1 to 5 having dimension equal to the number of grid points of the computational area. (INPUT)
6.	B	The numerator of the right side of Eq. (26). (OUTPUT)
7.	P	The vector given by Eq. (25). (OUTPUT)
8.	R	The vector given by Eq. (24). (OUTPUT)
9.	T1	Temporary storage.
10.	T2	Temporary storage.
11.	U3	Band 3 given by Eq. (21). (OUTPUT)
12.	X	Initial solution guess. (INPUT)
13.	Y	The right hand side Eq. (59). (INPUT)
14.	MN	The number of grid points. (INPUT)
15.	M	The number of radial grid points. (INPUT)

CALL CORICC (A1, A2, A3, A4, A5, B, P, R, T1, T2, U3, X, Y, MN, M, EPS).

The arguments for CORICC are the same as for SETICC with the following exceptions:

12.	X	The current solution.
16.	EPS	The sum of the squares of residuals.

The solution vector $\underline{X}$ typically is obtained by calling SETICC once and then repeatedly calling CORICC until EPS is sufficiently small.

The five band ICCG algorithm consumes a large fraction of the computational expense of solving the equilibrium problem. To implement ICCG efficiently on the Cray 1 computer, we have written subroutines SETICC, CORICC, BACKL, BACKU, DINV, and MATMUL in assembly language. The FORTRAN versions of these subroutines accept any values for MN and M, provided M exactly divides MN, mod (MN, M) = 0. The assembly language version has the same arguments for the user-called subroutines SETICC and CORICC, but it has two additional restrictions. The band-offset M must be greater than or equal to 8 and less than or equal to 64, 8 must exactly divide M, mod (M, 8) = 0 and mod (MN, 64) = 0. Assembly language versions of these subroutines may be written without these restrictions; however, it is not then possible to derive the maximum performance from the Cray 1 hardware. The restrictions arise from the optimization of two types of do loops. The method chosen to optimize these do loops depends on the presence of 64 words in each Cray 1 vector register.

The first type of do loop to be optimized is recursive and thus prevents complete vectorization by the CFT compiler.

```
      DO 20 I = MN - M, 1, - 1
20    X(I) = [Y(I) - A4(I) * X(I + 1) - A5(I) * X(I + M)]/A3(I)
```

Because array A3 is fixed the first optimization is achieved by replacing the divide by a multiply with T4(I) = 1.0/A3(I). To allow further partial vectorization two temporary arrays are introduced with two inner do loops. The innermost loop is vectorizable and the do loop overhead is further reduced by introducing eight statements for X(J).

```
      DIMENSION T5(M), T6(M)
      DO 20 I = MN - M, 1, - M
      DO 15 J = I, I - M + 1, - 1
      T5(I + 1 - J) = T4(J) * [Y(J) - A5(J) * X(J + M)]
```

```
15      T6(I + 1 - J) = T4(J) * A4(J)

        DO 20 J = I, I - M + 1, - 8

        X(J) = T5(I + 1 - J) - T6 (I + 1 - J) * X(J + 1)

        X(J - 1) = T5 (I + 1 - J - 1) - T6 (I + 1 - J - 1) * X(J)

        X(J - 2) = T5 (I + 1 - J - 2) - T6 (I + 1 - J - 2) * X(J - 1)

        X(J - 3) = T5 (I + 1 - J - 3) - T6 (I + 1 - J - 3) * X(J - 2)

        X(J - 4) = T5 (I + 1 - J - 4) - T6 (I + 1 - J - 4) * X(J - 3)

        X(J - 5) = T5 (I + 1 - J - 5) - T6 (I + 1 - J - 5) * X(J - 4)

        X(J - 6) = T5 (I + 1 - J - 6) - T6 (I + 1 - J - 6) * X(J - 5)

20      X(J - 7) = T5 (1 + 1 - J - 7) - T6 (I + 1 - J - 7) * X(J - 6)
```

Machine language programming permits careful reordering of the
instruction sequence, optimal use of parallel processing, and the subsequent
elimination of temporaries T5 and T6. An overall run time reduction from 4459
to 997 microseconds is achieved with MN = 4096, M = 64.

The second type of do loop to be optimized is not vectorizable by CFT as
written below.

```
        S = 0
        DO 20 I = 1, N
20      S = S + X(I) * X(I)
```

To permit vectorization this do loop is split into three loops as
follows.

```
        DIMENSION TEMP(64)
        S = 0
        DO 5 I = 1, 64
5       TEMP(I) = X(I) * X(I)
        DO 15 I = 65, N, 64
        DO 15 J = 1, 64
15      TEMP(J) = TEMP(J) + X(I + J - 1) * X(I + J - 1)
        DO 30 J = 1, 64
30      S = S + TEMP(J)
```

Only the last do loop does not vectorize. When the above FORTRAN is coded in assembly language, TEMP(I) is eliminated and an overall run time reduction from 1859 to 90 microseconds is achieved with N = 4096.

C. BOUNDARY VALUE GREEN'S FUNCTION

The Green's function is computed by subroutine GREENF. The Green's function over the entire grid for a given point is evaluated by a single call to GREENF. Symmetry across z = 0 is assumed and the Green's function is used with the right hand side of Eq. (1) so the output of GREENF is [G(r', z', r,z) + G(r', - z', r,z)]/r' with G(r', z', r,z) given by Eq. (31). The IMSL library or an equivalent must be invoked since this routine requires functions MMDELK and MMDELE to compute elliptic integrals of the first and second kind. The calling sequence and explanation of arguments follows.

CALL GREENF (RFAC, ZFAC, R, IRDIM, Z, IZDIM, GREENS)

1.	RFAC	Radial position r of Eq. (31). (INPUT)
2.	ZFAC	Axial position z of Eq. (31). (INPUT)
3.	R(IRDIM)	Radial grid array. (INPUT)
4.	IRDIM	Number of radial grid points. (INPUT)
5.	Z(IZDIM)	Axial grid array. (INPUT)
6.	IZDIM	Number of axial grid points. (INPUT)
7.	GREENS (IRDIM, IZDIM)	Array of Green's function values divided by R for (RFAC, ZFAC) at grid positions given by arrays R and Z. Due to symmetry the Green's function at ± Z are combined.

Values of flux are computed by using trapezoidal integration by subroutine GREENG. The current is assumed to be symmetric about Z = 0, so the Green's function combined by GREENF is appropriate. The calling sequence and arguments follow.

CALL GREENG (SI, GREENS, RDB, XJTHET, IRDIM, IZDIM).

1.	SI	Value of flux at r,z position used to compute Green's function array. (OUTPUT)
2.	GREENS (IRDIM, IZDIM)	Array of Green's function values combined for ± z and divided by r as computed by GREENF. (INPUT)
3.	RDB (IRDIM, IZDIM)	Array of grid cell areas in square centimeters. RDB(i, j) = [R(i + 1) − R(i)] · [z(j + 1) − z(j)]. (INPUT)
4.	XJTHET (IRDIM, IZDIM)	Array of 4π r/c times the current in statamps. (INPUT)
5.	IRDIM	Number of radial grid points. (INPUT)
6.	IZDIM	Number of axial grid points. (INPUT)

The Green's function at z divided by r at a single point is computed by subroutine GREENH. For a fixed point RFAC, ZFAC this is the routine repetitively called by GREENF to get the Green's function over the entire grid. The calling sequence and arguments are below.

CALL GREENH (G, RFAC, ZFAC, R, Z).

1.	G	1/R [G(R,Z, RFAC, ZFAC) + G(R, − Z, RFAC, ZFAC)]. (OUTPUT)
2.	RFAC	Radial position r of Eq. (31). (INPUT)
3.	ZFAC	Axial position z of Eq. (31). (INPUT)
4.	R	Radial current position. (INPUT)
5.	Z	Axial current position. (INPUT)

A boundary point value is computed by first calling GREENF and then calling GREENG with 4π r/c times the current. For a typical 64 × 64 grid there are 520,000 Green's function values.

D. HILL'S VORTEX

The Hill's vortex formulas are computed by calling subroutine HILLSI. Values are communicated through common block HILLV. The calling sequence and definitions of common block elements are given below.

COMMON/HILLV/A(45)

CALL HILLSI

A(1)	Flux value at which functions are desired. (INPUT)
A(2)	Volume Eq. (33). (OUTPUT)
A(3)	$d\psi/dV$ the inverse of Eq. (35). (OUTPUT)
A(4)	$d^2\psi/dV^2$ Eq. (39). (OUTPUT)
A(5)	$\langle 1/r^2 \rangle$ Eq. (42). (OUTPUT).
A(6)	$d/dV \langle 1/r^2 \rangle$ Eq. (44). (OUTPUT)
A(7)	K Eq. (40). (OUTPUT)
A(8)	dK/dV Eq. (41). (OUTPUT)
A(9)	$\langle r^2 \rangle$ Eq. (46). (OUTPUT)
A(10)	$d/dV \langle r^2 \rangle$ Eq. (48). (OUTPUT)
A(11)	$\langle 1/B^2 \rangle$ Eq. (50). (OUTPUT)
A(12)	$d/dV \langle 1/B^2 \rangle$ Eq. (52). (OUTPUT)
A(13)	$\langle B^2 \rangle$ Eq. (54). (OUTPUT)
A(14)	$d/dV \langle B^2 \rangle$ Eq. (55). (OUTPUT)
A(15)	$2/3 \beta$ Eq. (32). This is the value of the distant uniform vacuum field. (INPUT)
A(16)	$(6\beta/\delta)^{1/2}$ Eq. (32). Radial position at which $\psi = 0$ at $z = 0$. (INPUT)
A(17)	$6\gamma/\delta$ Eq. (32), the ratio of radial to axial separatrix distance squared, E. (INPUT).

A(18)   The number of angular grid points used with
                         Simpson's rule to compute functions. (INPUT)

A(19) to A(45)   Working space.

III. AVAILABILITY

A LIB library containing FORTRAN subroutines FLINAV, SETICC, CORICC,
DINV, BACKL, BACKU, MATMUL, GREENF, GREENG, GREENH, and HILLSI is obtained
with the following execute line on the MFE 7600: FILEM READ .3040
.PHYSICS EQTRAN. A LIB library containing a binary assembly language
replacement for SETICC, CORICC, DINV, BACKL, BACKU, and MATMUL is obtained
with the following execute line on the MFE Cray 1: RFILEM READ .3040
.PHYSICS BICCG. Library BICCG contains the binary file BICCG2 and the
assembly language listing LICCG2.

IV. REFERENCES

1. H. Grad, Survey of 1-1/2 D Transport Codes, Courant Institute, New York City, Report MF-93 (1978).

2. D. S Kershaw, "The Incomplete Cholesky-Conjugate Gradient Method for the Iterative Solution of Systems of Linear Equation," J. Comp. Phys. 26, 43 (1978).

3. W. R. Smythe, Static and Dynamic Electricity, (McGraw-Hill, New York, N. Y., 1968).

4. M. J. Hill, "On a Spherical Vortex," Phil. Trans. Royal Soc. (A), Part I, 214 (1894).

EON/js

Fig. 1. Flux as a function of r and z with distance scaled to the plasma radius: geometry is (a) prolate, (b) spherical, and (c) oblate corresponding to E values 0.5, 1 and 2, respectively.
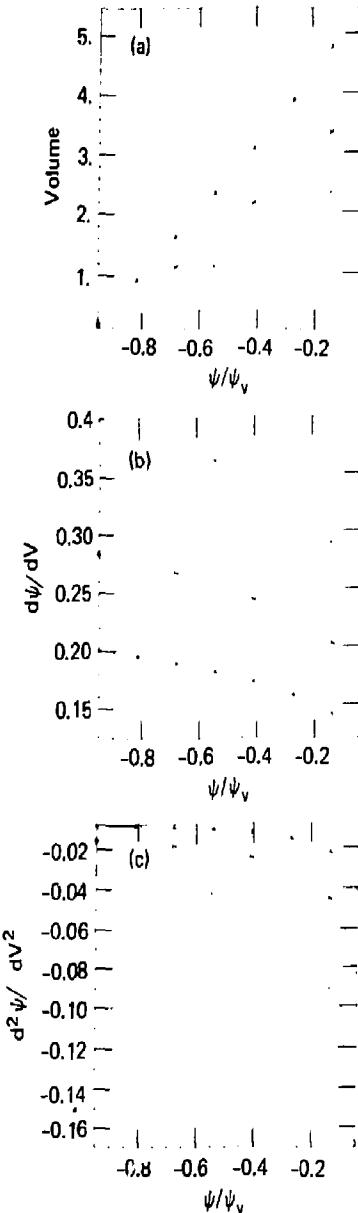
Fig. 2. Hill's vortex volume-related functions versus flux: (a) volume, (b) volume derivative of flux, and (c) second volume derivative of flux. Curves A, B, and C correspond to prolate, spherical and oblate geometry, respectively.
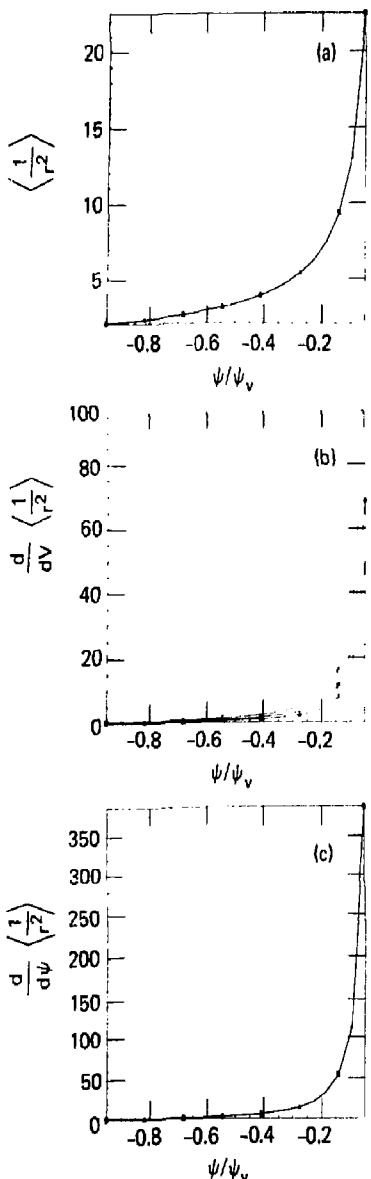
Fig. 3. Hill's vortex surface average of (a) $1/r^2$, $\langle 1/r^2 \rangle$, (b) the volume derivative of $\langle 1/r^2 \rangle$, and (c) the flux derivative of $\langle 1/r^2 \rangle$ as a function of normalized flux. Curves A, B, and C correspond to prolate, spherical and oblate geometry, respectively.
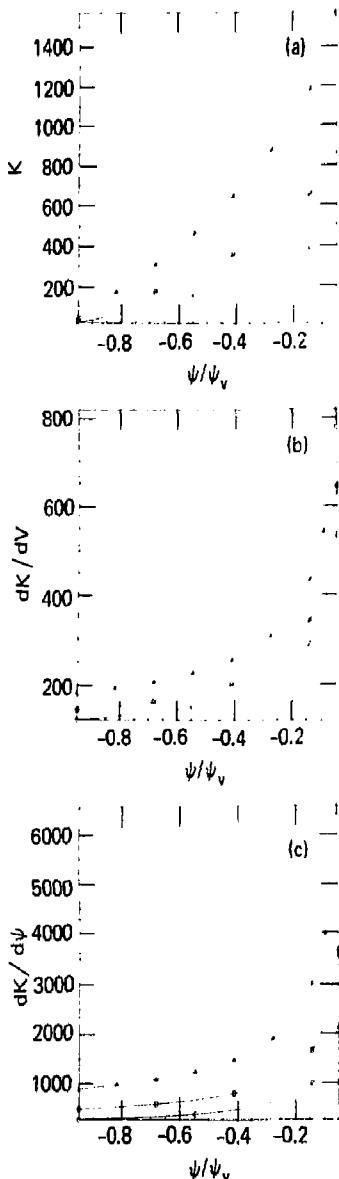
Fig. 4. Hill's vortex inductance: (a) K, (b) volume derivative of K, and (c) flux derivative of K. Curves A, B, and C correspond to prolate, spherical, and oblate geometry, respectively.
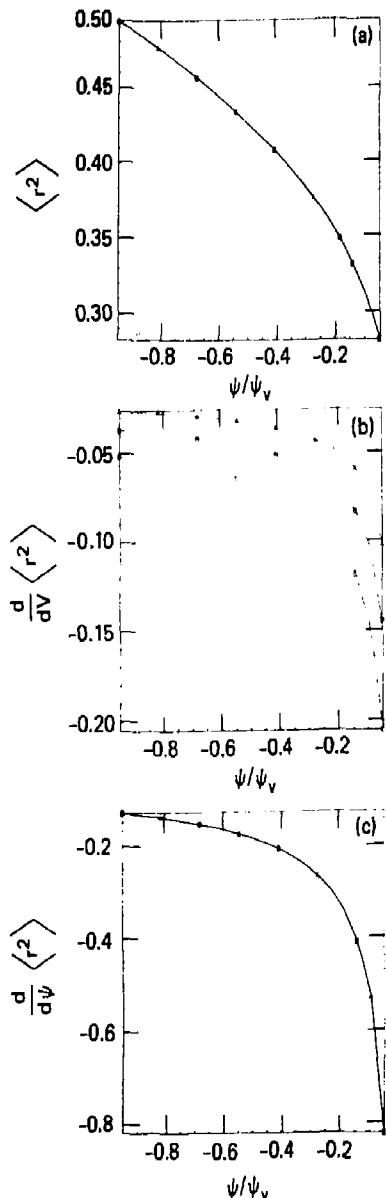
Fig. 5. Hill's vortex surface average of (a) r^2, $\langle r^2 \rangle$, (b) volume derivative of $\langle r^2 \rangle$, and (c) flux derivative of $\langle r^2 \rangle$. Curves A, B, and C correspond to prolate, spherical and oblate geometry, respectively.
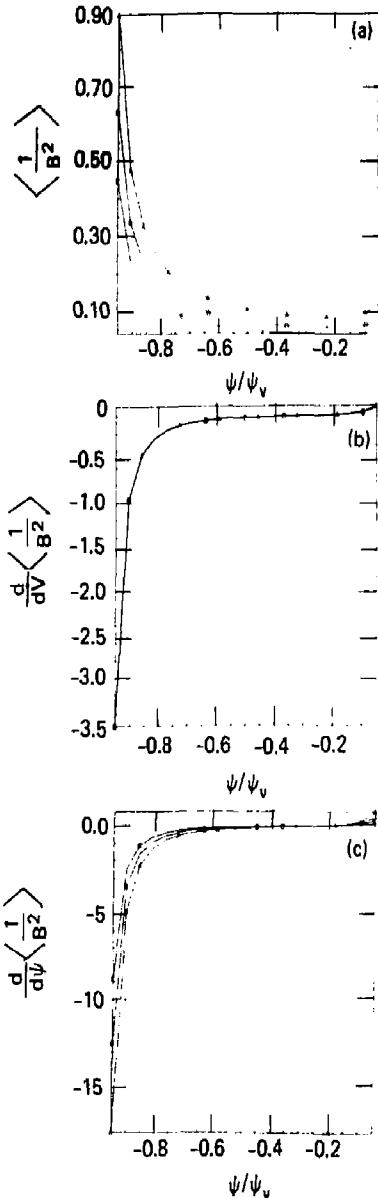
Fig. 6. Hill's vortex surface average of (a) $1/B^2$, $\langle 1/B^2 \rangle$, (b) the volume derivative of $\langle 1/B^2 \rangle$ and (c) the flux derivative of $\langle 1/B^2 \rangle$. Curves A, B, and C correspond to prolate, spherical and oblate geometry, respectively.
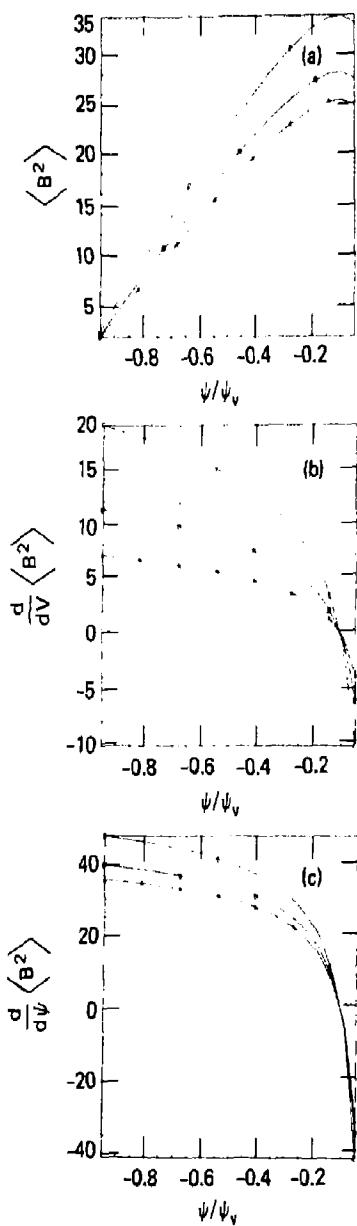
Fig. 7. Hill's vortex surface average of
(a) B^2, $\langle B^2 \rangle$, (b) the volume derivative of
$\langle B^2 \rangle$ and (c) the flux derivative of B^2.
Curves A, B, and C correspond to prolate,
spherical and oblate geometry, respectively.
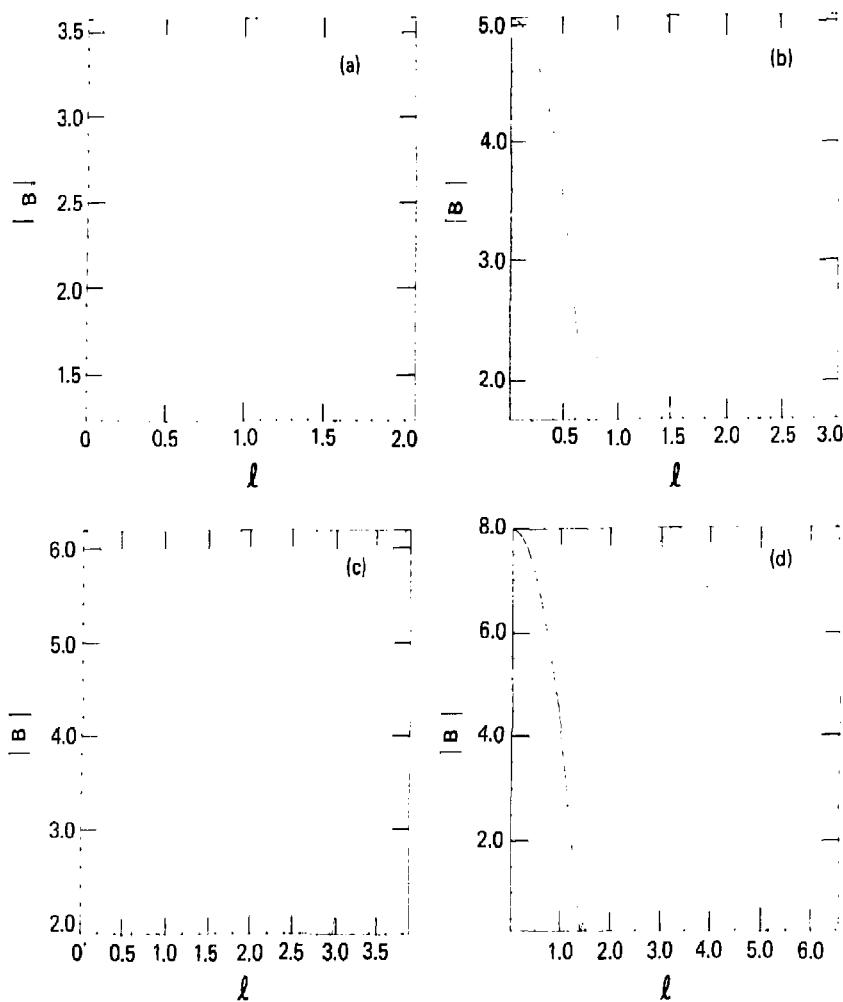
Fig. 8. Hill's vortex $|B|$ at (a) $\psi = -0.8$, (b) $\psi = -0.6$, (c) $\psi = -0.4$, and (d) $\psi = -0.0001$ versus clockwise distance, ℓ, around the constant ψ contour beginning at $z = 0$ beneath the vortex point, for the prolate geometry.
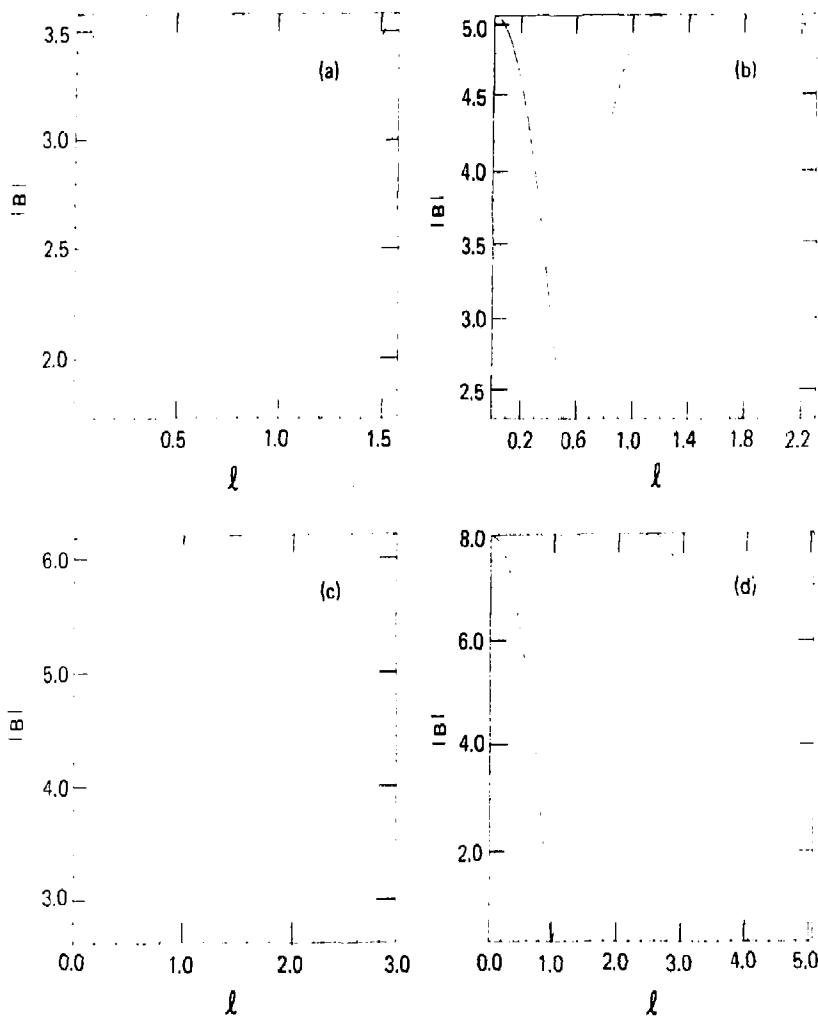
Fig. 9. Hill's vortex $|B|$ at (a) $\psi = -0.8$, (b) $\psi = -0.6$, (c) $\psi = -0.4$, and (d) $\psi = -0.0001$ versus clockwise distance, ℓ, around the constant ψ contour beginning at $z = 0$ beneath the vortex point for the spherical geometry.
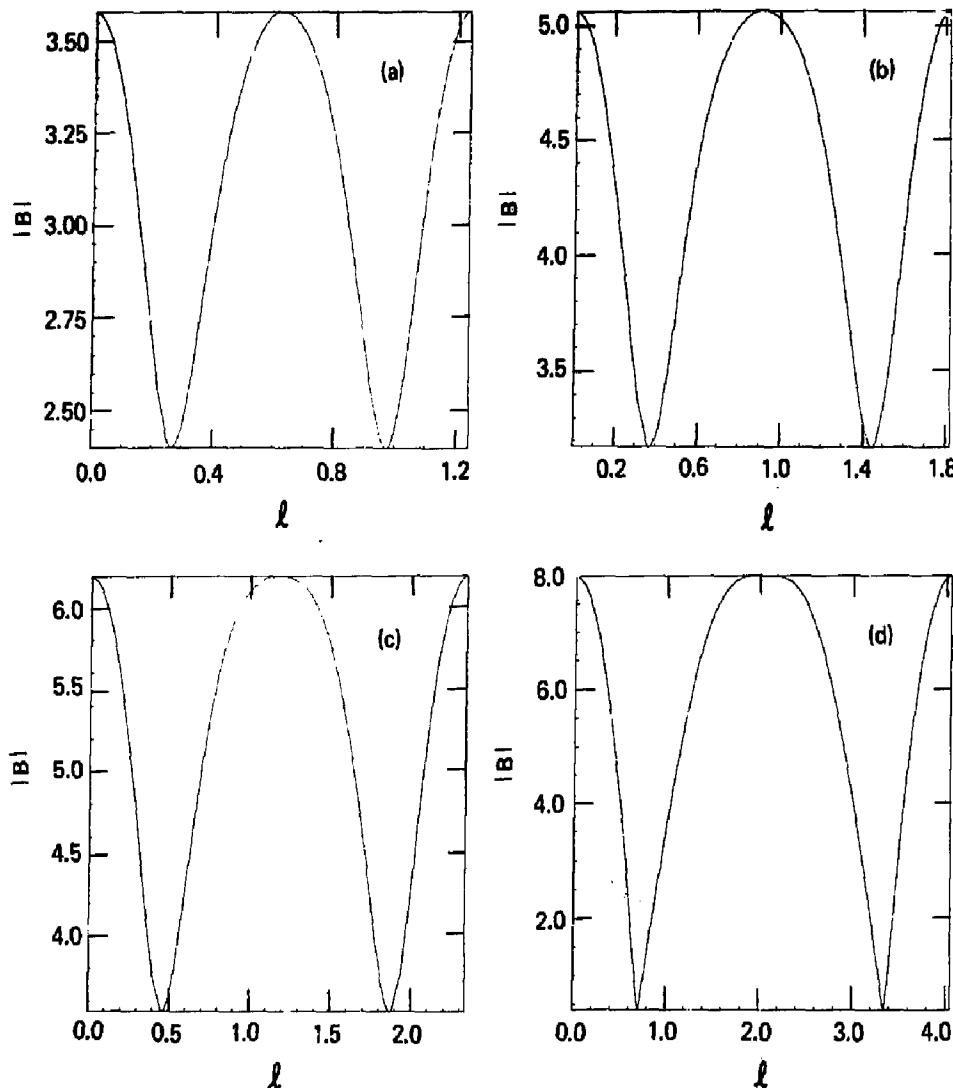
Fig. 10. Hill's vortex $|B|$ at (a) $\psi = -0.8$, (b) $\psi = -0.6$, (c) $\psi = -0.4$, and (d) $\psi = -0.0001$ versus clockwise distance, ℓ, around the constant ψ contour beginning at $z = 0$ beneath the vortex point for the oblate geometry.
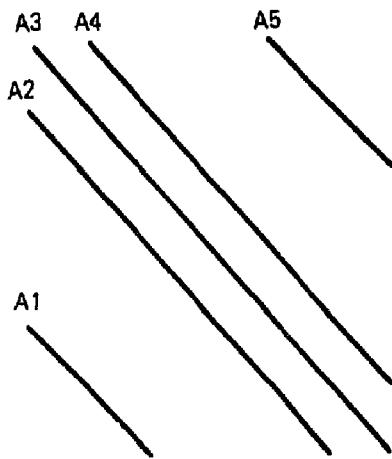
Fig. 11. Five band matrix structure.
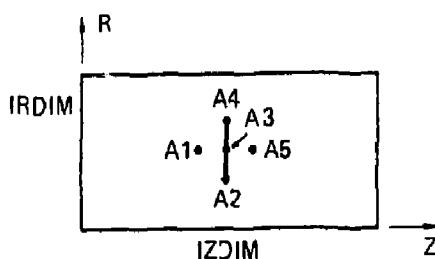
Fig. 12. The 2-D grid is dimensioned
IZDIM in the z direction and IRDIM in the
r direction. Matrix bands A1 to A5 are
indicated on the finite difference star.